Microstructure and Mechanical Properties of 316L Stainless Steel Fabricated Using Selective Laser Melting

SCHOLARONE™
Manuscripts

Microstructure and Mechanical Properties of 316L Stainless Steel Fabricated Using Selective Laser Melting

N. Iqbal[1], E. Jimenez-Melero[2], U. Ankalkhope[3], and J. Lawrence[1]

[1] *Institute for Advanced Manufacturing and Engineering, University of Coventry, CV6 5LZ, UK*

[2] *Materials Performance Centre, School of Materials, University of Manchester, M13 9PL, UK*

[3] *Manufacturing Technology Centre, Ansty Park, Coventry, CV7 9JU, UK*

ABSTRACT

The microstructure homogeneity and variability in mechanical properties of 316L stainless steel components fabricated using selective laser melting (SLM) have been investigated. The crack free, 99.9% dense samples were made starting from SS316L alloy powder, and the melt pool morphology was analysed using optical and scanning electron microscopy. Extremely fast cooling rates after laser melting/solidification process, accompanied by slow diffusion of alloying elements, produced characteristic microstructures with colonies of cellular substructure inside grains, grown along the direction of the principal thermal gradient during laser scanning. In some areas of the microstructure, a significant number of precipitates were observed inside grains and at grain boundaries. Micro hardness measurements along the build direction revealed slight but gradual increase in hardness along the sample height. Uniaxial tensile tests of as manufactured samples showed the effect of un-melted areas causing scatter in room-temperature mechanical properties of samples extracted from the same SLM build. The ultimate tensile strength (UTS) varied from 458MPa to 509MPa along with a variation in uniform elongation from 3.3% to 14.4%. The UTS of a sample exposed to the Cl- rich corrosion environment at 46ºC temperature revealed a similar strength as of the original sample, indicating good corrosion resistance of SLM samples under those corrosion conditions.

INTRODUCTION:

Selective Laser Melting (SLM) is an attractive additive manufacturing technique, receiving growing attention to produce 3D components with complex inner structures, in

a single-step building process [1, 2]. The process is based on the local melting of a pre-mixed metal alloy powder using a high power laser beam and layer-by-layer manufacturing of components, based on computer-aided design models. The technology offers the opportunity to manufacture components with unusual microstructures and properties due to multiple laser scan strategies and non-equilibrium solidification. It has been employed for materials across the board, from metals to polymers, ceramics to composites, and even more complex engineered materials [3-5]. The SS316L steel is among the widely used structural material due to combination of good mechanical properties and excellent corrosion resistance [6, 7]. Relatively recent studies have been carried out to improve the quality of SLM manufactured SS316L steel with optimum process conditions, to produce fully dense components with improved strength and ductility [8-10]. However, significant knowledge and experimental data is still needed to understand the formation of defects, pores, and microstructural heterogeneities intrinsic to the process, and to improve the performance for reliable structural components. This paper focuses mainly on the microstructural defects and their impact on the mechanical response of SS316L components produced by SLM. In particular, the specimens extracted from different locations of the same built were used to investigate the effect of defect distribution on the tensile behaviour of the material and failure mechanisms.

EXPERIMENTAL DETAILS

SLM Process

Cylindrical bars of diameter 14mm and height 125mm, were produced using a Renishaw AM250 system at National Centre for Additive Manufacturing (MTC, Coventry, UK). The precursor material was gas-atomized spherical SS316L powder, with a particle size ranging from 15 to 45 μm. The SLM process parameters were optimized at a layer thickness of 50 μm to minimize defect production and consequently ensure the dense bulk material. The platform was heated to 170°C from the beginning of the process and the temperature was maintained at the set level throughout the process. The samples were produced using a laser power of 200 W, with a laser spot size of 75μm and exposure time of 90μs. The hatch distance d_H was set to 90μm along with point distance d_P of 50μm, as shown in figure 1a.
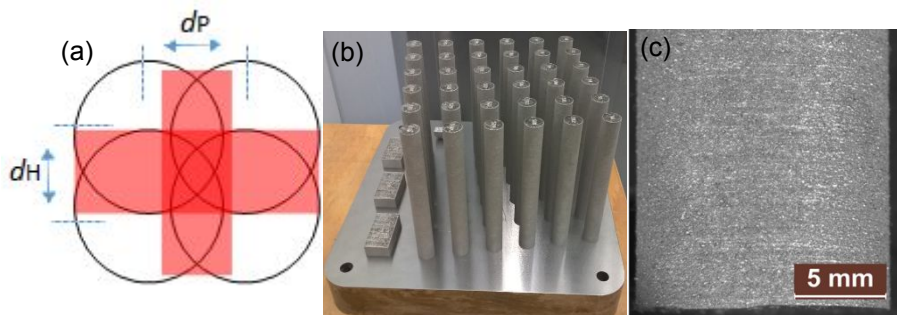

Figure 1. (a) Schematic of spot-to-spot melting process, (b) outlook of the as-built cylindrical bar samples, and (c) magnified view of the sample surface illustrating the scanning layers:

The layers were scanned using Chessboard strategy with island size of 5×5 mm, that involves the splitting of entire area into numerous local areas combined with a different scanning order [11]. This SLM strategy is considered beneficial to eliminate residual stresses and overheating of local areas. The as built samples are shown in figure 1b, with a magnified view of the sample surface shown in figure 1c.

Microstructure Characterization

The microstructure investigations of the samples extracted from the SLM build were carried out in an as-built condition. The samples were sliced parallel, as well as perpendicular to the long axis of the manufactured bar, mechanically ground and polished with a final step using suspension of colloidal silica. In order to reveal the microstructure, the samples were electro-etched in a solution containing 120 ml deionized water, along with 10% oxalic acid at a voltage of 5V for 60 seconds. Optical microscopy was used to characterize the resultant porosity. The average density of build samples was estimated by analyzing the porosity from multiple optical micrographs, based on the method reportedly successful for low porosity samples [12]. The grain morphology and fracture surfaces were analyzed using SEM.

Mechanical Testing

In order to investigate the effect of the microstructure heterogeneities on mechanical performance of the manufactured component, five dog-bone shape tensile specimens were extracted from the same single bar sample, using an EDM wire cutting process. Three tensile specimens were tensile tested according to BS EN ISO 6892-1 standards, while one tensile sample was exposed to corrosion environment using 5 vol.% NaCl solution for 10 days, at a temperature of 46°C, prior to uniaxial tensile testing at room temperature. One untested tensile sample was used for Vickers micro hardness (HV 0.5kg load) measurements along the gauge length of the sample to estimate the local mechanical properties.

RESULTS and DISCUSSION

Microscopic Porosity and Density

The optical micrographs from polished surfaces of a SLM sample are shown in figure 2. The micrographs revealed the presence of a limited number of micrometre sized pores inside the cross-section as well as side view of the bulk sample, as shown in figure 2a and 2b. However, few relatively large pores can also be seen in the side view, as shown in figure 2c. Certain level of porosity is intrinsic to the SLM process and cannot be completely avoided, as the gases trapped during manufacturing do not have enough time to surface out from the melt pool [13, 14]. The random distribution and spherical morphology of the observed pores illustrate that these pores are formed due to gas entrapment. Figure 2d shows the presence of some irregularly shaped voids, in few local areas. This is attributed to insufficient laser energy density during the scanning of that area, and represent un-melted zones [14]. Overall, the average density of the SLM sample,

calculated from image processing of optical micrographs taken from multiple locations was 99.9%.
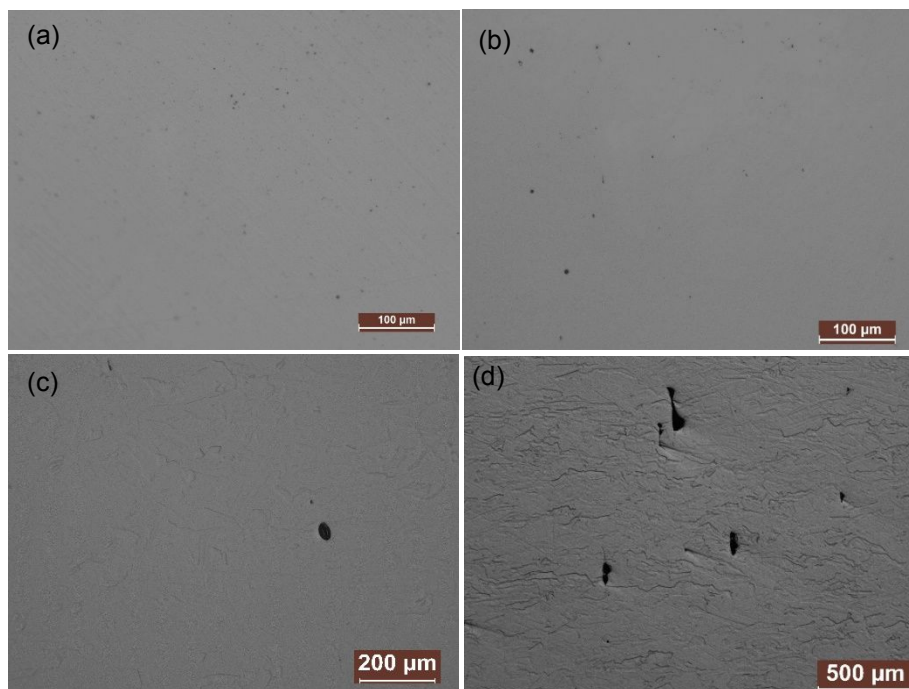

Figure 2. Optical micrograph from polished as-built SLM sample, (a) showing porosity in cross-section view, (b, c) in side view (build direction) and (d) typical irregularly shape defects.

Microstructure Characterization

The microstructure of the etched samples in the build direction is shown in figure 3. The optical micrographs clearly reveal the melt pool tracks. Previously melted and solidified melt pool zones are partially re-melted during scanning the next layer, leading to better consolidation and densification. The melt pools are observed to include multiple grains characterized by the same contrast, radially oriented within the melt pools. Many grains grew in multiple melt pools, in the direction of the main temperature gradient. The melt pools width was mostly larger than their depth, indicating conduction mode of melting. Overall, well merging of melt pools in figure 3a, illustrate that the laser energy density was sufficient to ensure the overlapping of adjacent melt pools to form a subsequent solid structure. However, a small number of defects are still observed at the melt pool boundaries, as shown in figure 3c. This represents lack of fusion in adjacent melt pools, which is confirmed by the presence of un-melted powder particles observed near the melt pool boundary. Randomly distributed precipitates were also observed at specific locations, both inside melt pool and at the melt pool boundaries as shown in figure 3d.

The higher magnification SEM images further revealed the presence of fine, needle shape, cellular substructure colonies, with different growth directions due to Chessboard scan strategy, as shown in figure 4a. Cellular microstructures have been previously reported

during laser welding when the solidification process experiences rapid cooling rates similar to SLM process [15,16]. The cells oriented in the same crystallographic orientation belong to the same grain, and usually cross the melt pool boundaries due to the partial re-melting involved.
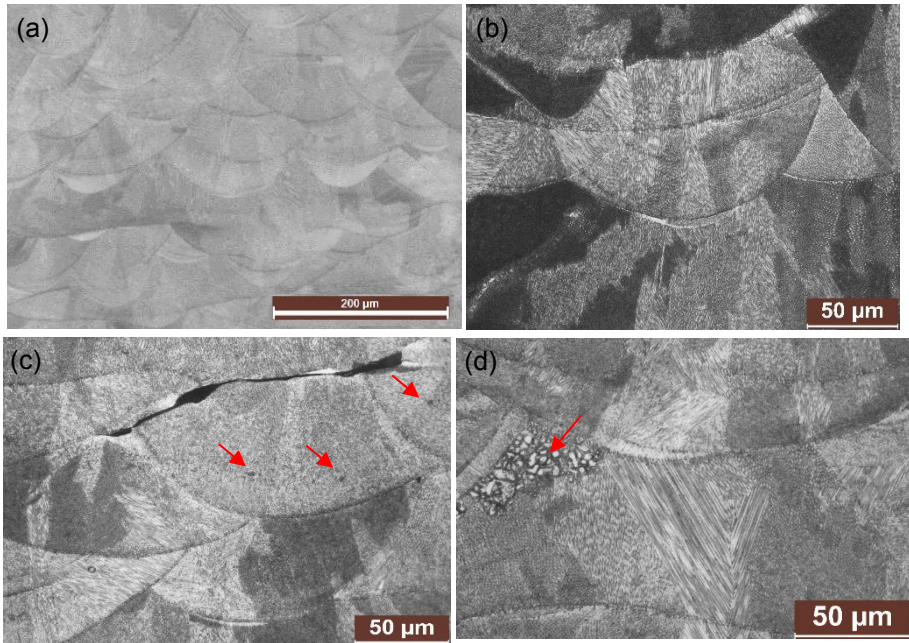
Figure 3. Etched surfaces of SLM sample. (a) Optical micrograph of the side view of melt pool assemblages, (b) multiple grains inside a melt pool illustrated by different contrast, (c) with lack of fusion defect and un-melted powder particles (arrows), and (d) with local precipitates (arrow) inside grains and at grain boundary

The magnified view of cellular growth inside grains of a melt pool is shown in figure 4b. No preferential orientation of grains is observed and the scan strategy used was able to avoid the formation of intense texture, resulting in an almost isotropic polycrystalline material. It was found that the cells always grew towards the melt pool boundary, with finer cell edges as shown in figure 4b. The EDX analysis in different regions of a cell did not shows any obvious difference in chemical composition. Therefore the variation in cell size towards the melt pool boundary should not be due to chemical variation but most probably due to difference in thermal conditions. The cell size usually depends on the temperature gradient that controls the growth rate. The temperature gradients at the melt pool boundary is expected to be quite sharp compared to the bulk melt pool, as that is close to the solidified sample making heat dissipation easier. As a result, the cells grow faster near the melt pool boundary, creating finer edges. Figure 4d indicates that the average cell diameter ranges from 2μm to 3μm, and with very high aspect ratios.
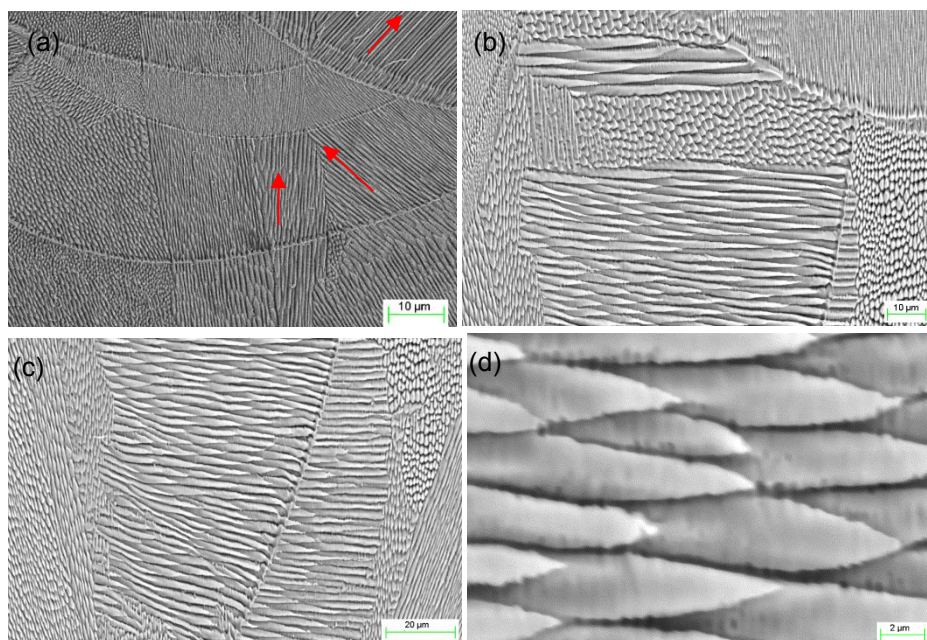
Figure 4. SEM micrographs of SLM sample. (a) Grains with cellular substructure growth along red arrows, in neighbouring melt pools, (b) grain entanglement within a melt pool, (c) cellular growth beyond melt pool boundary, and (d) magnified view of cells inside a grain.

Mechanical Testing

The tensile tests were performed on three specimens, in the as-built condition while one specimen was tensile tested after exposure to the Cl⁻ rich corrosion environment. Stress-strain curves along with images of fractured specimens are shown in figure 5a. A close view of the fractured specimens shows that the failure occurred at similar locations that constitute the upper half of the SLM specimen. However the UTS of the as-built tensile specimens S1, S3 and S4 varied significantly and was observed to be 477, 509 and 458 MPa respectively, with corresponding elongations of 3.3, 14.4 and 9.7%. The corrosion specimen S2 exhibited failure at UTS of 490 MPa and elongation 7.8%. The microscopic investigations of a polished sample after exposure to the Cl⁻ rich corrosion environment were also carried out and no traces of corrosion defects or pitting was observed. Table 1 compares the highest values of UTS and elongation observed in this study, with that reported in the literature, for SS316L produced through conventional processes. The performance of of SLM samples is relatively poor than the conventional materials. The microstructure of SLM specimen with Chessboard scan strategy did not show any preferred orientation of grains or cellular substructure that could explain the referenced variation in tensile behaviour. Rather the presence of fine cellular

microstructure with induced engineering grain boundaries is an important feature and expected to contribute to homogenous mechanical properties of SLM specimens.

Table 1: Mechanical properties of SS316L.

Material	UTS (MPa)	Elongation (%)	Reference
SLM	580	25.7	[17]
Forged	570	47.0	[18]
Wrought	620	53.0	[19]
SLM	509	14.4	[Our Study]

The micro-hardness profile across a tensile sample is shown in figure 5b, and also revealed no significant variations. The hardness slightly increased along the sample height, with average value 303HV, comparable to the values reported in the literature [20]. The fracture location was observed at the higher hardness zones. It was recognized that the marked variation in tensile strength and elongation of tensile specimens, could be the potential consequence of heterogeneous defects at different positions in the build.
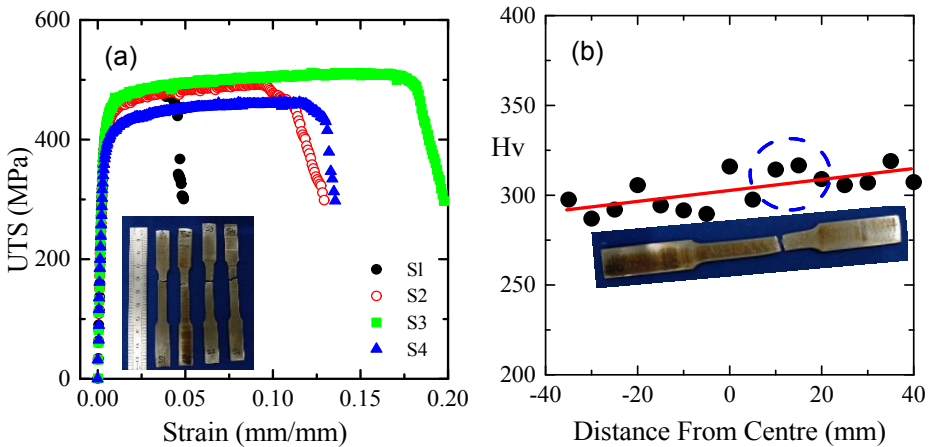

Figure 5. (a) Stress-strain curves for as-built tensile specimens S1, S3 and S4 along with corrosion specimen S2, and (b) variation in Vickers micro hardness across the sample height. The circle indicates the hardness at fracture location.

The fracture surface of the tested specimens was further investigated by SEM and representative images are shown in figure 6. Some discontinuous areas of varying size were detected on the fracture surface of tensile samples, with un-melted powder particles inside it. These are believed to be the fundamental cause of scatter in tensile properties. The clustering of these powder particles significantly reduces the effective cross-sectional area in tensile specimens, causing lower strength and ductility.
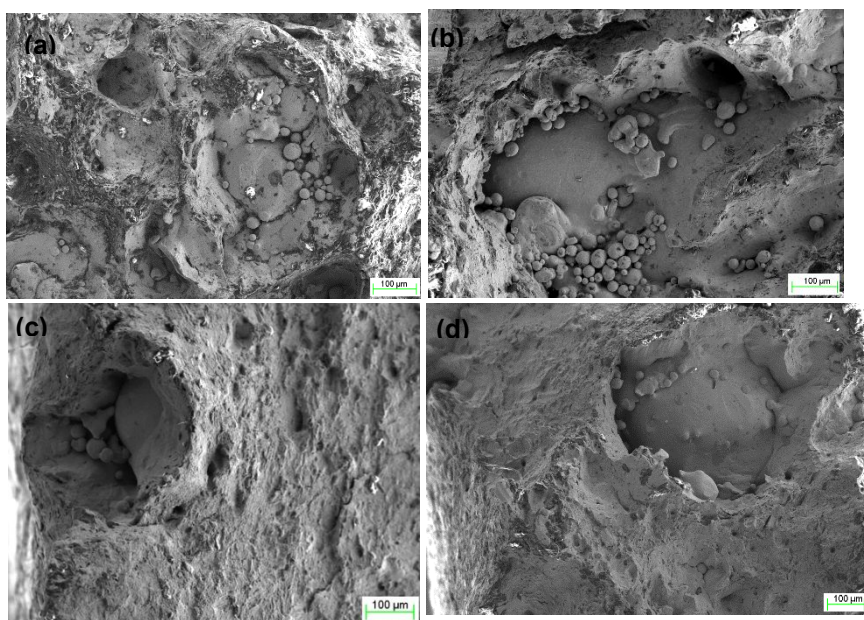
Figure 6. A magnified view of fracture surface of tensile specimens (a) S1, (b) S2, (c) S3 and (d) S4.

From present investigation, it is suggested that even for higher bulk density SLM components, the un-melted areas must be controlled through optimization of process parameters for improved strength and reliability.

CONCLUSIONS

The Chessboard scan strategy for SLM process is successfully employed to produce 99.9% dense SS316L specimens, with fine cellular microstructure, usually extending beyond the melt pool boundary. The mechanical testing exhibited marked scatter in the tensile strength and elongation. This is attributed to the presence of un-molten powder particles on the fracture surface of tensile specimens causing reduction in effective cross-sectional area. The tensile specimen exposed to the Chloride-rich corrosion environment did not show any significant effect on the tensile behaviour.

REFERENCES

1. D. Herzog, V. Seyda, E. Wycisk and C. Emmelmann, Acta. Matter. 117, 371 (2016)
2. D. Gu, W. Meiners, K. Wissenbach, and R. Poprawe, Int. Mater. Rev. 57, 133 (2012)
3. Y, Oh, C. Zhou, and S. Behdad, Additive Manufacturing, 22, 230 (2018)
4. W. Frazier, J. Mater. Eng. Perform., 23, 1917 (2014).
5. A. Simar, S. Godet and T. Watkins, Materials Characterization, 143, 1 (2018).
6. B. Qian and Z. Shen, J. Asian Ceram. Soc., 1, 315 (2013).
7. T. Lienert, P. Burgardt, K. Harada, R. Forsyth and T. DebRoy, Scr. Mater. 71, 35 (2014)
8. A. Riemer, S. Leuders, M. Thöne, H. Richard, T. Tröster and T. Niendorf, Eng. Fract. Mech., 120, 15 (2014).
9. B. Verlee, T. Dormal and J. Lecomte-Beckers, Powder Metall., 55, 260 (2012).
10. Y. Zhong, L. Liu, S. Wikman, D. Cui and Z. Shen, J. Nucl. Mater. 470, 170 (2016).

11. D. Koutny, D. Palousek, L. Pantelejev, C. Hoeller, R. Pichler, L. Tesicky, and J. Kaiser, Materials, *11*(2), 298 (2018).
12. A. Spierings and M. Schneider, and R. Eggenberger, Rapid Prototyping Journal 17(5), 380 (2011).
13. Y. Yang and H. Man, Surface and Coatings Technology, 132, 130 (2000).
14. H. Galarraga, D. A.Lados, R. Dehoff, M. Kirka and P. Nandwana, Additive Manufacturing, 10, 47 (2016).
15. S. Zhou, D. Chai, J. Yu, G. Ma, and D. Wu, Journal of Manufacturing Processes, 25, 220 (2017).
16. F. Verhaeghe, T. Craeghs, J. Heulens, L. Pandelaers, Acta. Mater., 57, 6006 (2009).
17. R. Casati, J. Lemke, M. Vedani, Journal of Materials Science & Technology, 32, 738 (2016).
18. M. Song, M. Wang, X. Lou, R. Rebak and G. Was, Journal of Nuclear Materials, 513, 33 (2019).
19. I. Segura, J. Mireles, D. Bermudez, C. Terrazas, L. Murr, K. Li, V. Injeti, R. Misra and R. Wicker , Journal of Nuclear Materials 507, 164 (2018).
20. K. Saeidi, X. Gao, Y Zhong, ZJ Shen, Materials Science and Engineering: A 625, 221 (2015).